International Communications in Heat and Mass Transfer 39 (2012) 657–664

Contents lists available at SciVerse ScienceDirect

International Communications in Heat and Mass Transfer

journal homepage: www.elsevier.com/locate/ichmt

A Peclet number based analysis of mixed convection for lid-driven porous square cavities with various heating of bottom wall ☆

Tanmay Basak [a,*], S. Roy [b], A.J. Chamkha [c]

[a] Department of Chemical Engineering, Indian Institute of Technology Madras, Chennai, 600036, India
[b] Department of Mathematics, Indian Institute of Technology Madras, Chennai, 600036, India
[c] Manufacturing Engineering Department, The Public Authority for Applied Education and Training, Shuweikh 70654, Kuwait

ARTICLE INFO

Available online 5 April 2012

Keywords:
Mixed convection
Square cavity
Porous medium
Uniform and non-uniform heating
Penalty finite element method
Peclet number

ABSTRACT

Mixed convection flows in a lid-driven square cavity filled with porous medium are studied numerically using penalty finite element analysis for uniform and non-uniform heating of bottom wall. The relevant parameters in the present study are Darcy number ($Da = 10^{-5} - 10^{-5}$), Grashof number ($Gr = 10^3 - 10^5$), Prandtl number ($Pr = 0.026 - 10$) and Reynolds number ($Re = 1 - 10^2$). The influence of convection is analyzed with Peclet number ($Pe = Re.Pr$). It is observed that the temperature profiles are symmetric for low values of Pe or Pr even in the presence of asymmetric flow fields irrespective of Da. The flow distribution affects significantly temperature distributions at high Pe irrespective of Da. Effect of Peclet numbers have been further investigated for both natural convection and forced convection dominant regimes at high Da. Strong coupling between flow fields and temperature are observed at high Pe. It is interesting to observe that large isothermal mixing zone at $Pr = 10$ reduces the overall flow strength compared to $Pr = 0.026$ case. Local Nusselt numbers show almost uniform and low values for low Peclet numbers and localized enhanced heat transfer rates are observed for high Peclet numbers at $Da = 10^{-3}$.

1. Introduction

In the recent years, mixed convection in porous media has received considerable attention because of its wide range of applications. A comprehensive review of the literature concerning convective flow in porous media may be found in the books by Nield and Bejan [1], Ingham and Pop [2], Vafai [3] and Bejan et al. [4].

Mixed convection studies are carried out in lid-driven cavity filled with porous medium for various applications [5–7]. Prasad and Koseff [5] performed many experiments in a lid-driven cavity filled with fluid to study the recirculation of mixed-convection flow. Their results indicate that the overall heat transfer rate is very weak function of Gr for $2200 \le Re \le 12{,}000$. Al-Amiri [6] analyzed numerically laminar transport processes in a lid-driven square cavity filled with a water-saturated porous medium. A stable thermal stratification configuration is considered by imposing a vertical temperature gradient. Kandaswamy et al. [7] studied numerically the mixed convection in a lid-driven square cavity filled with a fluid saturated porous medium and the governing equations are solved numerically by the finite volume method with the Semi Implicit Method for Pressure Linked Equation (SIMPLE) algorithm.

A few applications on mixed convection involve flow over vertical surface in porous medium [8-10]. Chamkha and Khaled [8] analyzed steady laminar hydromagnetic simultaneous heat and mass transfer by mixed convection flow over a permeable vertical plate immersed in a uniform porous medium. Steady mixed convection flow in a vented enclosure with an isothermal vertical wall and filled with a fluid-saturated porous medium is investigated by Mahmud and Pop [9]. Chin et al. [10] investigated the steady mixed convection boundary layer flow over a vertical impermeable surface embedded in a porous medium when the viscosity of the fluid varies inversely as a linear function of the temperature. A few other applications of mixed convection were also carried out by other investigators [11-16].

Till date, the role of flow fields on temperature distributions during mixed convection is poorly understood. The objective of this work is to present a generalized framework on understanding the flow and thermal coupling based on Peclet number. The case studies are considered for both uniform and non-uniform bottom heating of bottom wall. The specialty of the uniform and non-uniform bottom heating involves the realistic heating processes for practical applications. The non-uniform boundary conditions typically represented by sine functions, are found applications involving glass melting [17]. In the current study, Galerkin finite element method [18] with penalty parameter has been used to solve the nonlinear coupled partial differential equations governing flow and temperature fields. The detailed analysis of heat transfer rates or Nusselt numbers has been carried out using finite element basis functions.

☆ Communicated by W.J. Minkowycz.

* Corresponding author.
E-mail addresses: tanmay@iitm.ac.in (T. Basak), sjroy@iitm.ac.in (S. Roy), achamkha@yahoo.com (A.J. Chamkha).

0735-1933/$ – see front matter © 2012 Elsevier Ltd. All rights reserved.
doi:10.1016/j.icheatmasstransfer.2012.03.022

Nomenclature

Da	Darcy number
g	Acceleration due to gravity, m s^{-2}
k	Thermal conductivity, W m^{-1} K^{-1}
L	Length of the square cavity, m
K	Permeability, m^2
N	Total number of nodes
Nu	Local Nusselt number
p	Pressure, Pa
P	Dimensionless pressure
Pr	Prandtl number
Re	Reynolds number
Gr	Grashof number
T	Temperature, K
T_h	Temperature of hot bottom wall, K
T_c	Temperature of cold side walls, K
u	*x* component of velocity, m s^{-1}
U	*x* component of dimensionless velocity
U_0	*x* lid velocity, m s^{-1}
v	*y* component of velocity, m s^{-1}
V	*y* component of dimensionless velocity
X	Dimensionless distance along *x* coordinate
Y	Dimensionless distance along *y* coordinate

Greek symbols

α	Thermal diffusivity, m^2 s^{-1}
β	Volume expansion coefficient, K^{-1}
γ	Penalty parameter
θ	Dimensionless temperature
ν	Kinematic viscosity, m^2 s^{-1}
ρ	Density, kg m^{-3}
Φ	Basis functions
ψ	Streamfunction

2. Mathematical modeling and simulation

A schematic diagram of a two dimensional square porous cavity is displayed in Fig. 1 where the bottom wall is maintained at a uniform or non-uniform temperature. Vertical walls are kept at cold temperature and the top wall is well insulated. The top wall is assumed to slide from left to right with constant speed U_0. It is assumed that the solid matrix of the porous media does not undergo deformation and the porous bed is also assumed to be homogeneous, isotropic, saturated with incompressible fluid. All the thermophysical properties of the fluid such as viscosity, thermal conductivity, specific heats, thermal expansion coefficient and permeability except the density variation in the buoyancy term are considered to be constant. The Boussinesq approximation is considered for the fluid properties based on the variation of density with temperature and to couple the temperature field to the flow field. It is also assumed that the temperature of the fluid phase is equal to the temperature of the solid phase within the porous region, and local thermal equilibrium (LTE) is applicable in the present investigation [1]. Also, a velocity square term could be incorporated in the momentum equations to model the inertia effect which is more important for non-Darcy effect on the convective boundary layer flow over the surface of a body embedded in a high porosity media. However, we have neglected this term in the present study because we deal with the mixed convection flow in a cavity filled with a porous medium. Under these assumptions and neglecting the Forchheimer inertia term, the governing equations for steady two-dimensional mixed convection flow in a lid driven porous square cavity using conservation of mass, momentum and energy can be written with the following dimensionless variables or numbers

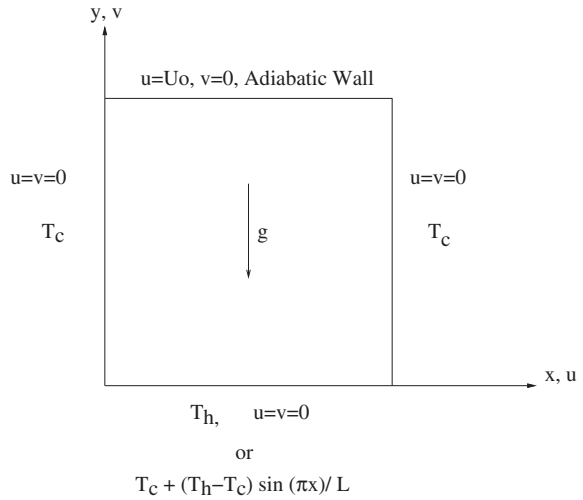

Fig. 1. Schematic diagram of the physical system.

$$\frac{\partial U}{\partial X}+\frac{\partial V}{\partial Y}=0, \tag{1}$$

$$U\frac{\partial U}{\partial X}+V\frac{\partial U}{\partial Y}=-\frac{\partial P}{\partial X}+\frac{1}{Re}\left(\frac{\partial^2 U}{\partial X^2}+\frac{\partial^2 U}{\partial Y^2}\right)-\frac{1}{Re\ Da}U, \tag{2}$$

$$U\frac{\partial V}{\partial X}+V\frac{\partial V}{\partial Y}=-\frac{\partial P}{\partial Y}+\frac{1}{Re}\left(\frac{\partial^2 V}{\partial X^2}+\frac{\partial^2 V}{\partial Y^2}\right)-\frac{1}{Re\ Da}V+\frac{Gr}{Re^2}\theta, \tag{3}$$

$$U\frac{\partial \theta}{\partial X}+V\frac{\partial \theta}{\partial Y}=\frac{1}{Re\ Pr}\left(\frac{\partial^2 \theta}{\partial X^2}+\frac{\partial^2 \theta}{\partial Y^2}\right). \tag{4}$$

The transformed boundary conditions are:

$$U(X,1)=1, U(X,0)=U(0,Y)=U(1,Y)=0,$$

$$V(X,0)=V(X,1)=V(0,Y)=V(1,Y)=0,$$

$$\theta(X,0)=1 \text{ or } sin(\pi X),$$

$$\theta(0,Y)=\theta(1,Y)=0, \frac{\partial \theta}{\partial Y}(X,1)=0. \tag{5}$$

The following dimensionless variables and parameters have been used in Eqs. (1)–(5):

$$X=\frac{x}{L}, Y=\frac{y}{L},\ U=\frac{u}{U_0}, V=\frac{v}{U_0}, \theta=\frac{T-T_c}{T_h-T_c},$$

$$P=\frac{p}{\rho U_0^2},\quad \Pr=\frac{\nu}{\alpha},\quad Da=\frac{K}{L^2},\quad \mathrm{Re}=\frac{U_0 L}{\nu},\quad Gr=\frac{g\beta(Th-T_c)L^3}{\nu^2} \tag{6}$$

The momentum and energy balance equations [Eqs. (2)–(4)] have been solved using the Galerkin finite element method. The continuity equation [Eq. (1)] is used as a constraint due to mass conservation and this constraint may be used to obtain the pressure distribution. In order to solve Eqs. (2)–(3), we use the penalty finite element method where the pressure (P) is eliminated by a penalty parameter, γ and the incompressibility criteria given by Eq. (1) (see [18]) results in

$$P=-\gamma\left(\frac{\partial U}{\partial X}+\frac{\partial V}{\partial Y}\right). \tag{7}$$

The continuity equation [Eq. (1)] is automatically satisfied for large values of γ. Typical values of γ that yield consistent solutions are 10^7. Using Eq. (7), the momentum balance equations [Eqs. (2) and (3)] reduce to

$$U\frac{\partial U}{\partial X}+V\frac{\partial U}{\partial Y}=\gamma\frac{\partial}{\partial X}\left(\frac{\partial U}{\partial X}+\frac{\partial V}{\partial Y}\right)+\frac{1}{Re}\left(\frac{\partial^2 U}{\partial X^2}+\frac{\partial^2 U}{\partial Y^2}\right)-\frac{1}{Re\ Da}U, \tag{8}$$

and

$$U\frac{\partial V}{\partial X}+V\frac{\partial V}{\partial Y}=\gamma\frac{\partial}{\partial Y}\left(\frac{\partial U}{\partial X}+\frac{\partial V}{\partial Y}\right)+\frac{1}{Re}\left(\frac{\partial^2 V}{\partial X^2}+\frac{\partial^2 V}{\partial Y^2}\right)-\frac{1}{Re\ Da}V+\frac{Gr}{Re^2}\theta. \tag{9}$$

The system of equations [Eqs. (4), (8) and (9)] with boundary conditions [Eq. (5)] are solved by using Galerkin finite element method [18] using the following expansions:

$$U\approx\sum_{k=1}^{N}U_k\ \Phi_k(X,Y),\quad V\approx\sum_{k=1}^{N}V_k\ \Phi_k(X,Y),\quad \text{and}\quad \theta\approx\sum_{k=1}^{N}\theta_k\ \Phi_k(X,Y), \tag{10}$$

The numerical solutions obtained in terms of the velocity components (U, V) and streamfunctions (ψ) are evaluated using the relationship between the streamfunction (ψ) and the velocity components [19], where the streamfunction (ψ) is defined in the usual way as $U=\frac{\partial\psi}{\partial Y}$ and $V=-\frac{\partial\psi}{\partial X}$. It may be noted that, the positive sign of ψ denotes anticlockwise circulation and the clockwise circulation is represented by the negative sign of ψ. The no-slip condition is valid at all boundaries as there is no cross flow, hence $\psi=0$ is used for the boundaries except the moving top wall. The heat transfer coefficient in terms of the local Nusselt number (Nu) is defined by

$$Nu=-\frac{\partial\theta}{\partial n}, \tag{11}$$

where n denotes the normal direction on a plane. The local Nusselt numbers at bottom wall (Nu_b) and at the side wall (Nu_s) are defined as:

$$Nu_b=\sum_{i=1}^{9}\theta_i\frac{\partial\Phi_i}{\partial Y}\quad\text{and}\quad Nu_s=\sum_{i=1}^{9}\theta_i\frac{\partial\Phi_i}{\partial X}. \tag{12}$$

Note that, the derivative in Eq. (11) is evaluated at a node on the walls based on element basis functions. A node typically belongs to an element and nine elemental basis functions are required to evaluate derivatives within a bi-quadratic element as shown in Eq. (12).

3. Results and discussion

3.1. Numerical tests

The computational domain consists of 28×28 bi-quadratic elements which correspond to 57×57 grid points. The bi-quadratic elements with lesser number of nodes smoothly capture the non-linear variations of the field variables which are in contrast with finite difference/finite volume solution available in the literature [20,21]. In order to establish accuracy of our numerical procedure, we have also tested our algorithm based on current grid size for driven cavity flow and mixed convection [20,21]. The results are in good agreement with previous simulation results [21] and the comparisons are not shown for the brevity of the manuscript. To ensure the convergence of the numerical solution to the exact solution, the grid sizes have been optimized following a similar manner of an earlier work [22] and the results presented here are independent of grid sizes.

The present finite element approach offers special advantage on evaluation of local Nusselt number at the bottom and side walls as the element basis functions are used to evaluate the heat flux. The numerical accuracy on the average Nusselt numbers and maximum horizontal and vertical dimensionless velocity components at an assigned vertical and horizontal plane across the cavity are within 0.1–1%.

3.2. Spatial distributions of temperature and flow: role of various parameters

Results are shown for various parameters such as Darcy number (Da), Prandtl number (Pr), Grashof number (Gr) and Reynolds number (Re). The ranges of Da are within $10^{-5}-10^{-3}$ for the simulations. Three representative values of Pr such as 0.026 (molten metal), 0.7 (air) and 10 (water) are considered for the simulation. Intensity of mixed convection is governed by Gr and Re. An important parameter, Richardson number ($Ri=\frac{Gr}{Re^2}$) is often used for analysis on mixed convection. In general, $Ri\approx0$ indicates dominance of forced convection whereas $Ri\approx\infty$ denotes dominance of natural convection. Role of convection on thermal characteristics is governed by Peclet number ($Pe=Re.Pr$) which is the ratio between heat transfer by convection and heat transfer by conduction. The flow and temperature fields are strongly coupled or the convective heat transport is dominant if Peclet number ($Pe=Re.Pr$) is high.

Effect of Darcy numbers, Prandtl numbers, Grashof numbers will be discussed next. The variations of flow configurations and coupling with temperature profile will be illustrated further based on various limits of Pe. Spatial flow fields and temperature distributions are shown for uniform heating of bottom wall and the qualitatively similar distributions for non-uniform heating of bottom wall are omitted for the brevity of the manuscript.

3.2.1. Effect of Darcy number

Simulations were carried out for $Pr=0.026$, $Re=1$ and $Gr\le10^5$ for various values of Da and it is found that conduction dominant heat transport occurs and the flow field does not influence isotherms (figures not shown).

Fig. 2 shows the effect of Darcy number for $Pr=10$, $Re=100$, $Pe=10^3$ and $Gr=10^5$. Fig. 2(a) shows that the primary circulation occupies most of the cavity and strength of circulation is weak as maximum value of streamfunction is 0.002 at $Da=10^{-5}$. It is interesting to observe that, flow characteristics couple with temperature distributions at higher Pr limit. Based on energy balance equation (Eq. (4)), it may be inferred that Peclet number ($Pe=RePr$) is sufficiently high ($Pe=10^3$) to induce convective effect on temperature distributions. However, intensity of flow and temperature are not strongly coupled at a smaller Da to increase heating rate at the top portion of the cavity. Although at high Pe, convective heat transport is found to occur, but heat cannot penetrate towards the top wall due to lower thermal diffusivity at $Pr=10$. In addition, flow intensity is quite less at low Da ($Da=10^{-5}$). Thus, a large thermal gradient near the bottom wall is observed whereas a large zone near the top wall is maintained at $\theta\le0.1$ at larger Pr.

As the Darcy number increases to 10^{-4}, the flow intensity for both primary and secondary circulations become gradually stronger. It is interesting to observe that at higher Pr ($Pe=10^3$), the zone of secondary circulations is shortened and the zone of primary circulations increases (see Fig. 2(b)). Due to larger intensity of convective transport at high Pe and at $Da=10^{-4}$, isotherms are now found to be highly coupled with flow fields. Consequently, due to smaller thermal diffusivity, the larger thermal gradients are observed near the left and bottom walls whereas a large zone near the right wall is still maintained at $\theta=0.1$. Further increase of Da to 10^{-3} in Fig. 2(c) shows the dominant effect of forced flow based on single primary circulation cell accompanied with tiny secondary cell at the left corner.

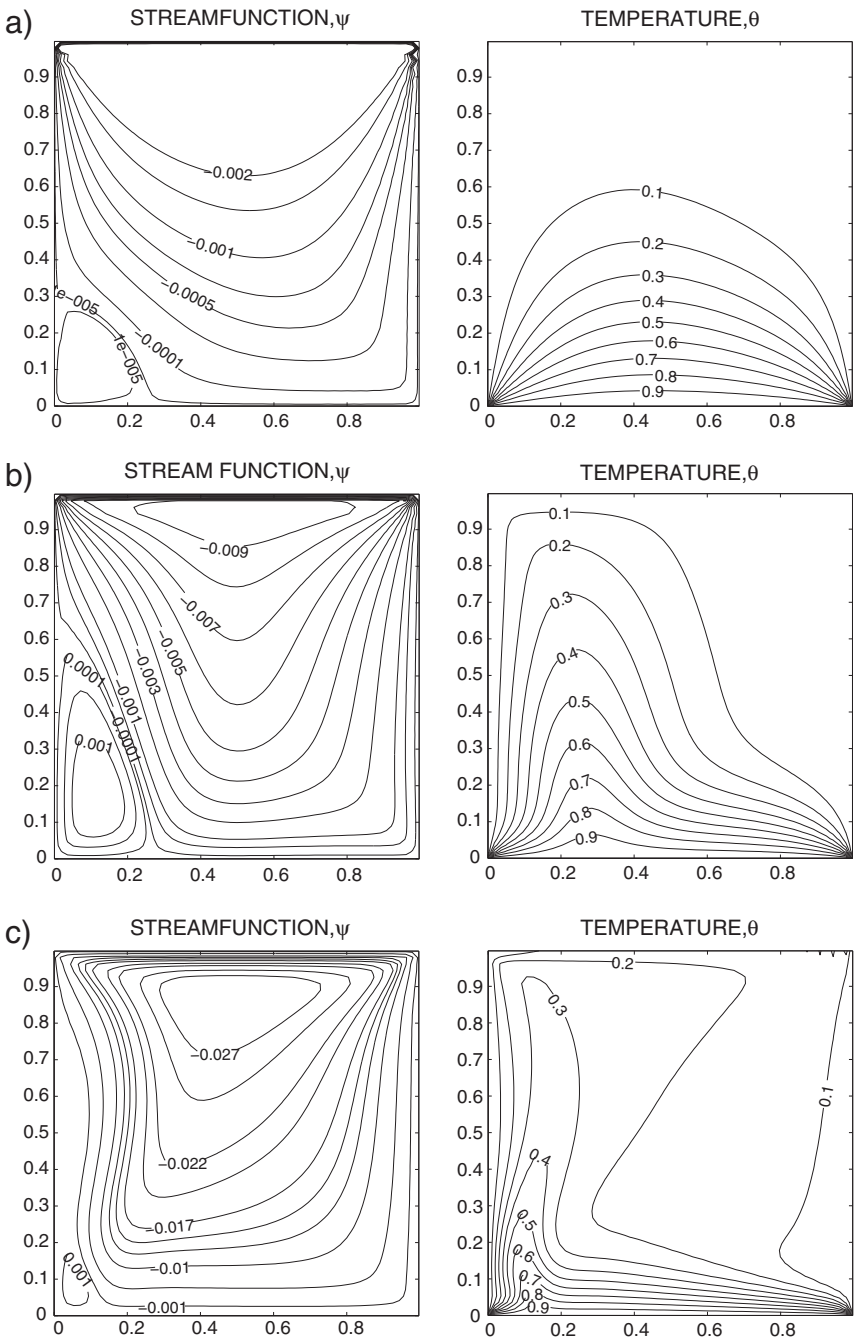

Fig. 2. Streamfunction and temperature contours for uniform heating of bottom wall with $Pr = 10$, $Re = 100$, $Pe = 10^3$, $Gr = 10^5$: (a) $Da = 10^{-5}$ (b) $Da = 10^{-4}$ and (c) $Da = 10^{-3}$.

The lid velocity causes cooler fluid to flow along the right wall from the top wall. Thus, more than 70% of the cavity associated with right wall is maintained at $\theta \leq 0.2$ whereas the compressed isotherms with $\theta \geq 0.3$ are found near the left and bottom walls due to high value of Pr ($Pr = 10$). It is interesting to observe that strength of convection is significant for $Da = 10^{-3}$ and 10^{-4} at larger Pe ($Pe = 10^3$) with $Re = 10^2$.

3.2.2. Effect of Prandtl number, Reynold number and Peclet number

Analysis has been carried out to study streamlines and isotherms for various Pr (Pe) with $Da = 10^{-3}$ with two limits of Reynolds numbers ($Re = 10, 100$) at $Gr = 10^5$. The results are shown at a representative high Da ($Da = 10^{-3}$) and $Gr = 10^5$ to study the role of flow fields on thermal characteristics. Results are not shown for $Re = 1$ as the qualitative trends on streamlines and isotherms for $Re = 1$ are similar to those for $Re = 10$. It may be noted that the flow circulation cells are almost symmetric signifying natural convection dominance for $Re \leq 10$ with various Pr (0.026, 0.7 and 10) whereas forced convection plays significant role for higher values of $Re (> 10)$.

Fig. 3a–c illustrates distributions on streamlines and isotherms at $Re = 10$ for $Gr = 10^5$ with various Pr. The mixed convection is found to be less significant at $Re = 10$ or $Ri = 10^3$ for all Pr (Pe) as seen from Fig. 3a–c. It is found that two sets of oppositely rotating circulation cells occur in each half of the cavity and the right circulation cells expand further near the top wall due to dominance of lid velocity. The effect of convection for various Pr on the temperature field may be explained based on Peclet numbers for each Pr.

Flow field and temperature profiles are found to be decoupled and conduction dominant heat transport is observed for $Pr = 0.026$ ($Pe = 0.26$). Therefore, temperature profiles are found to be symmetric

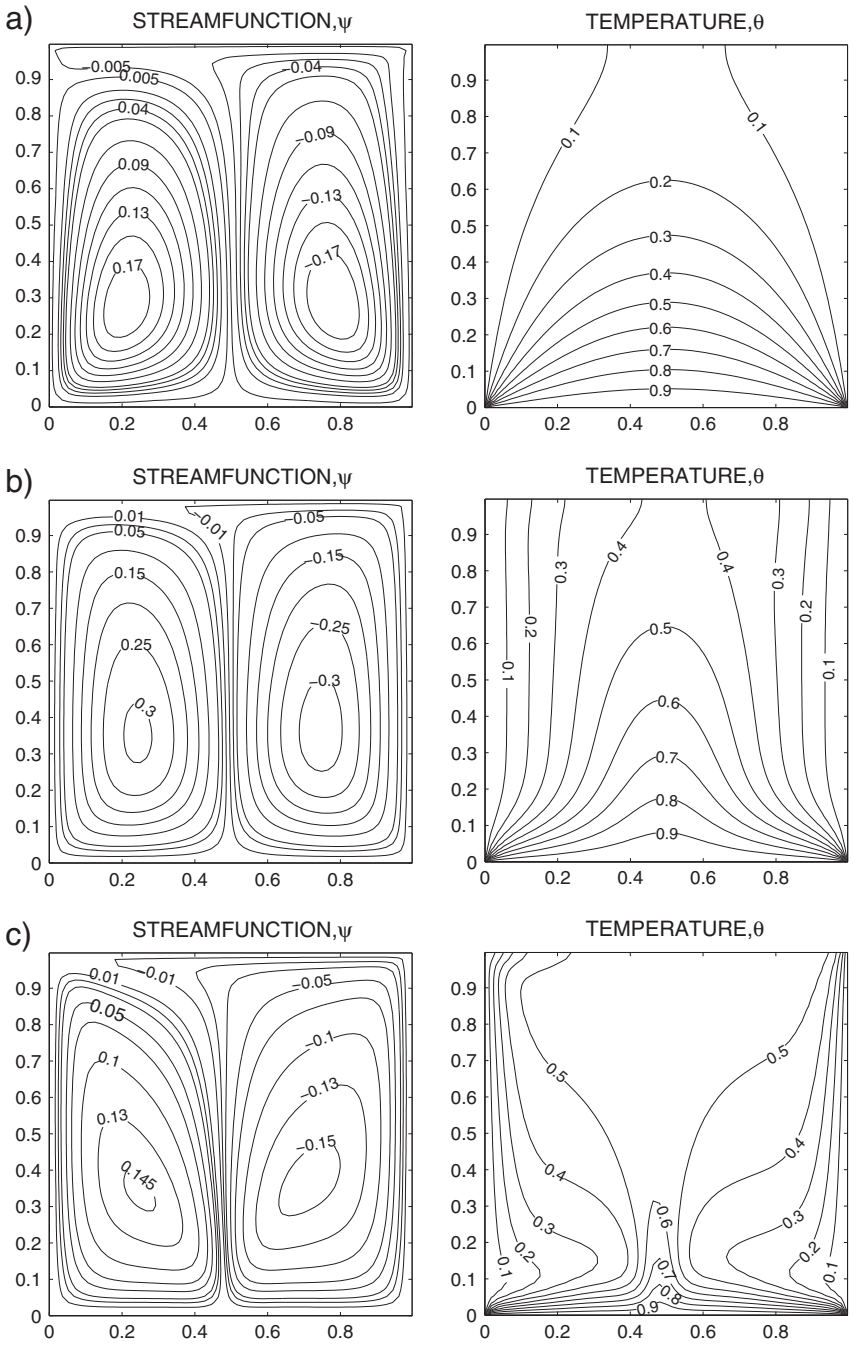

Fig. 3. Streamfunction and temperature contours for uniform heating bottom wall with $Re = 10$, $Gr = 10^5$, $Da = 10^{-3}$: (a) $Pr = 0.026$ ($Pe = 0.26$) (b) $Pr = 0.7$ ($Pe = 7$) and (c) $Pr = 10$ ($Pe = 10^2$).

inspite of asymmetric flow fields as seen in Fig. 3a. Intensity of convection is increased as Pr increases to 0.7. It may be noted that $|\psi|_{max} \approx 0.17$ for $Pr = 0.026$ while $|\psi|_{max} \approx 0.3$ for $Pr = 0.7$. Due to significant effect of forced convection, the cell size at the right portion for specific $|\psi|$ values is slightly larger than that at the left portion of the cavity. The strong thermal boundary layer is found to develop along the side walls due to counter rotating flow cells at larger Pr (see Fig. 3b and c). Also, the thermal boundary layer is developed near the bottom wall. The isotherms along the centerline take the shape of the plume due to strong upward flow based on counter rotating cells induced by hot bottom wall. Note that, the flow and temperature fields are strongly coupled at a high Pe ($Pe = 7$) as seen in Fig. 3b.

The effect of flow on the temperature distribution can be viewed as the result at higher Pe ($Pe = 100$) with $Pr = 10$ and enhanced thermal mixing due to enhanced convection occurs near the central zone where a large portion is maintained at $\theta = 0.5 - 0.6$. It is interesting to note that the thermal boundary layer thickness near the top portion of side walls is much smaller than those cases with smaller Pr values. These phenomena in turn affect the flow field. Due to enhanced thermal mixing, at the central zone, buoyancy effect is negligible along the central zone. As a result, the flow induced by natural convection is lesser due to less thermal gradient induced by thermal mixing. Thus the flow due to natural convection would not add a significant contribution to the flow field induced by lid velocity. Overall, the resultant flow strength is found to be even smaller than that with $Pr = 0.026$ and that can be seen from $|\psi|_{max}$ values (see Fig. 3a–c).

Fig. 4a–c display flow and temperature distributions for $Re = 100$ and $Gr = 10^5$ at various Pr. Fig. 4a shows the distributions for

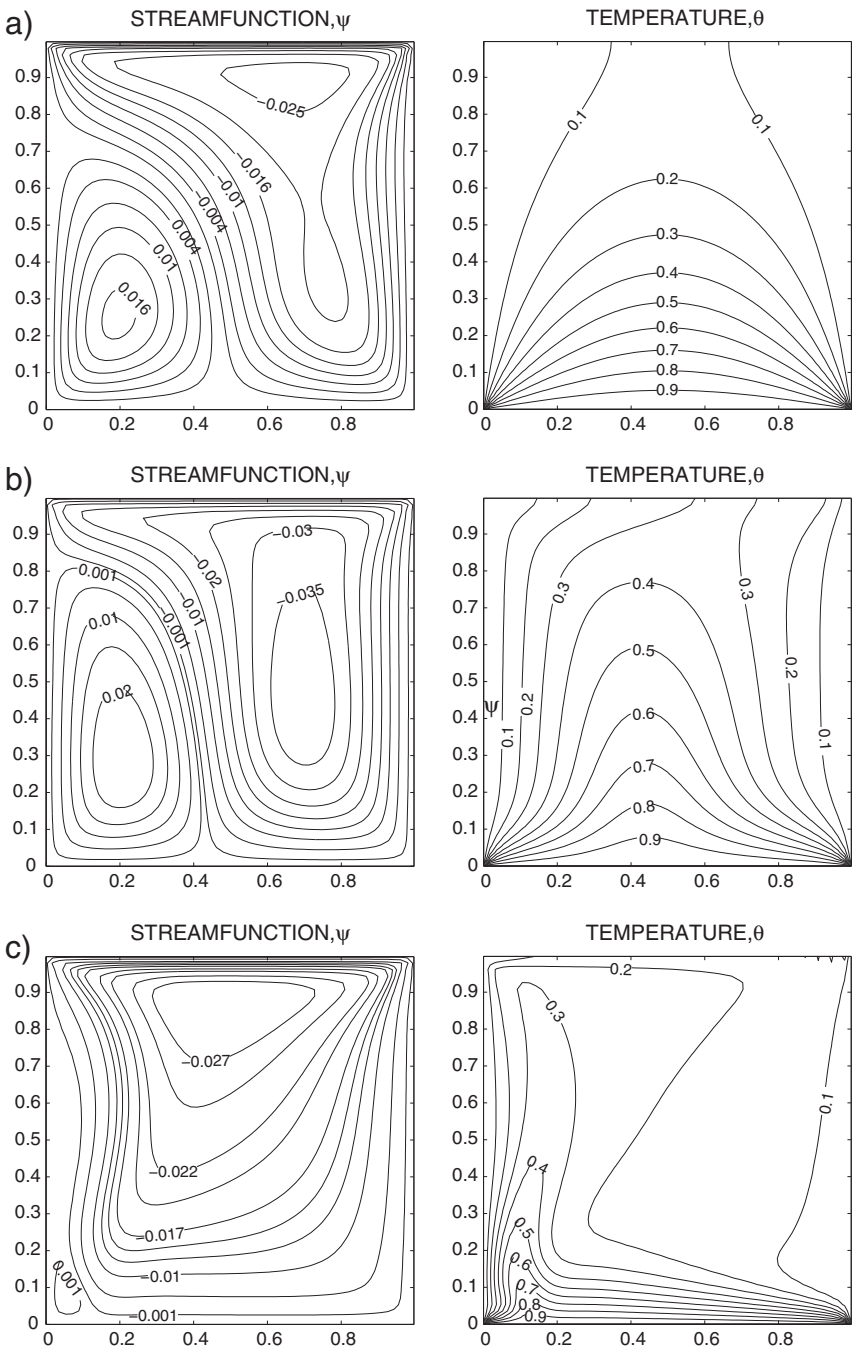

Fig. 4. Streamfunction and temperature contours for uniform heating of bottom wall with $Re=100$, $Gr=10^5$, $Da=10^{-3}$: (a) $Pr=0.026$ ($Pe=2.6$) (b) $Pr=0.7$ ($Pe=70$) and (c) $Pr=10$ ($Pe=10^3$).

$Pr=0.026$. The dominant effect of lid velocity is observed based on larger flow circulation near the right wall. Small secondary circulation cell is observed near the left corner of the bottom wall. The secondary circulation near the left corner is due to weak buoyancy effect at $Ri=1$. It is interesting to observe that temperature profiles are smooth and symmetric based on conduction dominant heat transport at $Pr=0.026$ and $Re=100$ ($Pe=2.6$). The flow characteristics are found to follow similar qualitative trend as Pr increases to 0.7. But, the flow intensities of both primary and secondary cells are found to be increased. It is found that $|\psi|_{max}$ is around 0.035 for $Pr=0.7$ whereas that is 0.025 at $Pr=0.026$. It is interesting to observe that the flow field is strongly coupled with heat transport at a high Peclet number ($Pe=70$). The lid velocity plays a dominant role and the temperature profile is found to be asymmetric (see Fig. 4b). The stronger clockwise circulation cell near the right wall leads to greater thermal mixing near the right half. In addition, the circulation cell near the left wall is weaker. Therefore, the thermal mixing is weak near the left wall and stronger thermal boundary layer is found to be developed near the left wall.

A single clockwise primary circulation cell accompanied by a tiny secondary cell around the left corner is found to occur at $Pr=10$ (see Fig. 4c). The convective heat transport is dominant at a high Peclet number ($Pe=10^3$). The fluid is cooler near the top wall and thus cold fluid is recirculated in the zone near the top wall around the center of vortex which corresponds to $|\psi|_{max}\approx 0.27$. Thus temperature varies within 0.2–0.3 at a large central zone. Due to the clockwise flow, the cold fluid flows down along the right wall. Consequently, the temperature near the right wall is maintained around 0.1. On

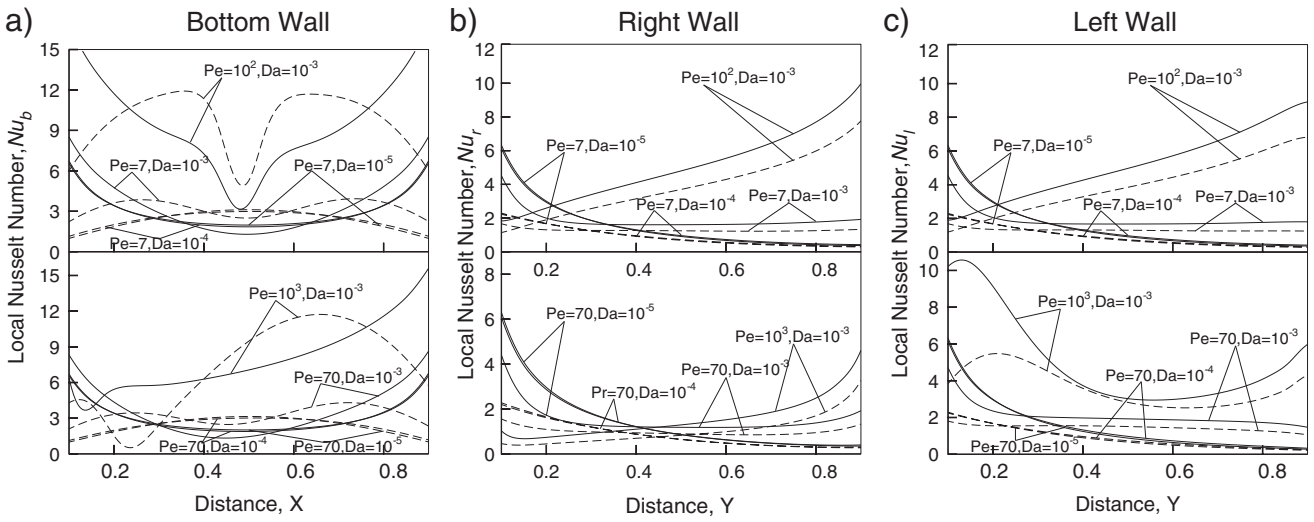

Fig. 5. Variation of Local Nusselt Number with the distance at the (a) bottom wall (b) right wall and (c) left wall for uniform heating (−) and non-uniform heating (…) of bottom wall for $Gr = \mathbf{10^5}$. In each plot, upper panel corresponds to $Re = 10$ and lower panel represents $Re = 10^2$.

the other hand, the weak fluid flow along the left wall keeps the fluid warm and a highly compressed boundary layer is formed. These features are also shown in Fig. 2c. In addition, strong thermal boundary layers along the bottom and left walls are due to smaller thermal diffusivity at higher *Pr*. Similar to earlier cases, dominant effect on convective heat transport reduces the local buoyancy effect and the flow strength with $Pr = 10$ ($Pe = 10^3$) is found to be smaller than that with $Pr = 0.7$ ($Pe = 70$).

3.3. Heat transfer rates: Nusselt numbers

Fig. 5(a), (b) and (c) demonstrate the effect of *Da* ($10^{-5} - 10^{-3}$) on spatial distribution of the local Nusselt numbers at the bottom, right and left walls (Nu_b, Nu_r and Nu_l), respectively with $Pr = 0.7$ and 10 at $Re = 10$ (upper panel) and 10^2 (lower panel). The thermal gradient values represent typically magnitudes of Nusselt numbers. Due to the presence of discontinuity in the temperature boundary conditions at the edges of bottom wall, the local heat transfer rate (Nu_b) at edges is very high irrespective of all Darcy and Prandtl numbers for uniform heating of bottom wall [upper panel of Fig. 5(a)]. The temperature profile is found to be symmetric at $Re = 10$ ($Ri = 10^3$) representing dominance of natural convection. In general, large portion of the bottom wall corresponds to Nu_b with similar order of magnitudes at low *Pe*. At high *Pe* ($Pe = 10^2$), convection strongly couples with temperature distributions and isotherms are highly compressed at the bottom all resulting in larger values of Nu_b. Asymmetric distributions of Nu_b are observed for mixed convection dominance regime ($Re = 100, Ri = 10$) (see the bottom panel of Fig. 5a). High values of Nu_b are observed at the right half of bottom wall both for uniform and non-uniform heating cases. Trends of Nu_r and Nu_l are qualitatively similar for $Re = 10$ corresponding to dominance of natural convection (see upper panels of Fig. 5b, c). The local Nusselt numbers are quite low for non-uniform heating cases especially for smaller values of *Pe*. However, the Nusselt numbers are quite large at the top portion of side walls due to high thermal gradient based on strong coupling with flow distributions at high *Re*. Similar to $Re = 10$, the Nusselt number distributions are quite small for both uniform and non-uniform heating cases with $Pe < 70$ and $Re = 10^2$. Due to prominent mixed convection effect at $Re = 10^2$, the distributions of Nu_r and Nu_l are different (see bottom panels of Fig. 5b, c). It is interesting to observe that Nu_l is quite high at the lower half for $Pe = 10^3$. In general, both the Nu_l and Nu_r values are larger for uniform heating cases for all Peclet numbers, but Nu_b exhibits larger values for the central zone of the bottom wall due to non-uniform heating. Average Nusselt numbers were found to follow a power law relationship with *Gr* for various Peclet numbers and detail variations are not shown for the brevity of the manuscript.

4. Conclusions

The influence of uniform and non-uniform heating of the bottom wall on the flow and heat transfer characteristics due to lid driven mixed convection flow within a square cavity filled with porous medium has been studied in the present investigation. Role of convection on temperature distributions are assessed via the concept of Peclet number (*Pe*).

It is observed that at low Darcy number ($Da = 10^{-5}$), the isotherms are smooth and monotonic for all the *Gr*, *Pr* and *Re*. It is also interesting to observe that the isotherms are found to be symmetric signifying negligible effect of lid velocity while processing low *Pr* fluid, corresponding to smaller values of *Pe*, irrespective of *Da* even at high *Gr* and *Re*. The natural and forced convection effects are prominent at higher *Da* ($Da = 10^{-3}$). However, the presence of natural or forced convection is determined from *Pr*, *Re* and *Gr*. Simulation results are shown for three representative values of *Pr* (0.026, 0.7 and 10) for various values of *Re* (10 and 100) at $Gr = 10^5$. The effect of mixed convection on the temperature distributions is further quantified by Peclet number (*Pe*). It is found that the temperature distributions are almost symmetric for $Re = 10$ with low *Pr* fluid even with asymmetric flow fields. The significant effect of lid velocity is observed at $Re = 100$ and $Pr = 10$ ($Pe = 10^3$). It is interesting to observe that the flow intensity is reduced for $Pr = 10$ due to less intensity of buoyancy caused by large isothermal cold fluid in the cavity. Qualitatively similar spatial temperature and flow patterns were observed for uniform and non-uniform heating of bottom wall.

Spatial distribution of Nusselt numbers is shown for two representative fluids ($Pr = 0.7$ and 10) with a high value of *Gr* ($Gr = 10^5$). It is found that Nusselt numbers are quite small and less variations are found with distance for low Peclet numbers. Interesting results on local heat transfer rates are found for high Peclet number and Reynolds number for mixed convection dominant regimes.

References

[1] D.A. Nield, A. Bejan, Convection in porous media, 3rd edn Springer, Berlin, 2006.
[2] D.B. Ingham, I. Pop (Eds.), Transport Phenomena in Porous Media, Elsevier, Oxford, 2005.
[3] K. Vafai, Handbook of porous media, second ed., Taylor and Francis, New York, 2005.

[4] A. Bejan, I. Dincer, S. Lorente, A.F. Miguel, A.H. Reis, Porous and complex flow structures in modern technologies, Springer, New York, 2004.
[5] A.K. Prasad, J.R. Koseff, Combined forced and natural convection heat transfer in a deep lid-driven cavity flow, International Journal of Heat and Fluid Flow 17 (1996) 460–467.
[6] A.M. Al-Amiri, Analysis of momentum and energy transfer in a lid-driven cavity filled with a porous medium, International Journal of Heat and Mass Transfer 43 (2000) 3513–3527.
[7] P. Kandaswamy, M. Muthtamilselvan, J. Lee, Prandtl number effects on mixed convection in a lid-driven porous cavity, Journal of Porous Media 11 (2008) 791–801.
[8] A.J. Chamkha, A.R.A. Khaled, Nonsimilar hydromagnetic simultaneous heat and mass transfer by mixed convection from a vertical plate embedded in a uniform porous medium, Numerical Heat Transfer Part A-Applications 36 (1999) 327–344.
[9] S. Mahmud, I. Pop, Mixed convection in a square vented enclosure filled with a porous medium, International Journal of Heat and Mass Transfer 49 (2006) 2190–2206.
[10] K.E. Chin, R. Nazar, N.M. Arifin, I. Pop, Effect of variable viscosity on mixed convection boundary layer flow over a vertical surface embedded in a porous medium, International Communications in Heat and Mass Transfer 34 (2007) 464–473.
[11] T.C. Jue, Analysis of flows driven by a torsionally–oscillatory lid in a fluid-saturated porous enclosure with thermal stable stratification, International Journal of Thermal Sciences 41 (2002) 795–804.
[12] S. Jaballah, R. Bennacer, H. Sammouda, A. Belghith, Numerical simulation of mixed convection in a channel irregularly heated and partially filled with a porous medium, Journal of Porous Media 11 (2008) 247–257.
[13] O. Aydin, A. Kaya, Mixed convection of a viscous dissipative fluid about a vertical flat plate embedded in a porous medium: constant heat flux case, Journal of Porous Media 11 (2008) 207–217.
[14] J. Ghazanfarian, A. Abbassi, Mixed convection in a square cavity filled with a porous medium and different exit port position, Journal of Porous Media 10 (2007) 701–718.
[15] K.C. Wong, N.H. Saeid, Numerical study of mixed convection on jet impingement cooling in a horizontal porous layer-using Brinkman-extended Darcy model, International Journal of Thermal Sciences 48 (2009) 96–104.
[16] S.V.S.S.N.V.G.K. Murthy, B.V.R. Kumar, Non-Darcy mixed convection in a porous square enclosure under suction/injection effects with a non-isothermal vertical wall, Numerical Heat Transfer PART A-Applications 57 (8) (2010) 580–602.
[17] I.E. Sarris, I. Lekakis, N.S. Vlachos, Natural convection in a 2D enclosure with sinusoidal upper wall temperature, Numerical Heat Transfer Part A-Applications 42 (5) (2002) 513–530.
[18] J.N. Reddy, An introduction to finite element analysis, McGraw-Hill, New York, 1993.
[19] G.K. Batchelor, An Introduction to Fluid Dynamics, Cambridge University Press, 1993.
[20] R. Schreiber, H.B. Keller, Driven cavity flows by efficient numerical techniques, Journal of Computational Physics 49 (1983) 310–333.
[21] M.K. Moallemi, K.S. Jang, Prandtl number effects on laminar mixed convection heat-transfer in a lid-driven cavity, International Journal of Heat and Mass Transfer 35 (1992) 1881–1892.
[22] M.M. Ganzarolli, L.F. Milanez, Natural-convection in rectangular enclosures heated from below and symmetrically cooled from the sides, International Journal of Heat and Mass Transfer 38 (1995) 1063–1073.